CW Operation of a Tunable 1550-nm VCSEL Integrating Liquid-Crystal Microcells

Benjamin Boisnard, Christophe Levallois, Cyril Paranthoen, Salvatore Pes, Thierry Camps, Benattou Sadani, Karine Tavernier, Sophie Bouchoule, Laurent Dupont, Mehdi Alouini, et al.

▶ **To cite this version:**

Benjamin Boisnard, Christophe Levallois, Cyril Paranthoen, Salvatore Pes, Thierry Camps, et al.. CW Operation of a Tunable 1550-nm VCSEL Integrating Liquid-Crystal Microcells. IEEE Photonics Technology Letters, 2020, 32 (7), pp.391-394. 10.1109/LPT.2020.2975076 . hal-02876673

HAL Id: hal-02876673
https://hal.science/hal-02876673

Submitted on 21 Jun 2020

HAL is a multi-disciplinary open access archive for the deposit and dissemination of scientific research documents, whether they are published or not. The documents may come from teaching and research institutions in France or abroad, or from public or private research centers.

L'archive ouverte pluridisciplinaire **HAL**, est destinée au dépôt et à la diffusion de documents scientifiques de niveau recherche, publiés ou non, émanant des établissements d'enseignement et de recherche français ou étrangers, des laboratoires publics ou privés.

CW Operation of a Tunable 1550-nm VCSEL Integrating Liquid-Crystal Microcells

B. Boisnard, C. Levallois, C. Paranthoen, S. Pes, T. Camps, B. Sadani, K. Tavernier, S. Bouchoule, L. Dupont, M. Alouini, P. Debernardi, and V. Bardinal

***Abstract*— An InP-based Vertical-Cavity Surface-Emitting Laser (VCSEL) with a liquid crystal (LC) microcell monolithically integrated on its surface for spectral tuning is investigated. Unlike tunable VCSELs integrating a movable membrane, here the physical length of the cavity remains unchanged and only the voltage applied on the LC ensures a refractive index modification for a particular polarization emitted by the VCSEL. This tunable VCSEL operates in CW at room temperature and exhibits more than 23 nm wavelength tuning around 1.55 μm at a maximum applied voltage of 20 V. The measured laser threshold around 6.5 mW is still comparable to VCSEL without LC microcell, a clear indication that the optical losses related the LC are very low. On the other hand, for this first optically pumped device, the lasing characteristics suggest that the LC birefringence is lower than expected. To assess this hypothesis, thermo-optical simulations have been conducted.**

***Index Terms*— Vertical-cavity surface-emitting lasers, liquid crystal devices, semiconductor lasers.**

I. Introduction

VERTICAL-CAVITY Surface-Emitting Lasers (VCSELs) are key optical sources for optical communications, and more recently for applications like autofocus imaging or facial recognition on smartphones [1]. Their well-known advantages related to longitudinal single-mode emission, circular beam shape with a low divergence, low-power consumption, and an easy 2D integration for mass production are very attractive for such applications. However, for a wider range of applications, including gas sensing [2], Optical Coherence Tomography (OCT) [3], [4], Fiber Bragg Grating (FBG) sensing [5] and optical spectroscopy [6], wavelength tunability is required. In this case, the large free spectral range related to the VCSEL microcavity becomes interesting to obtain a wide spectral tunability without mode hopping. To realize such tunable VCSEL, it is then required to change the optical length of the cavity. The most used technique is based on the variation of the physical length of the optical resonator. This is typically achieved by thermal or electrostatic actuation of a suspended membrane acting as a movable end mirror for the cavity, which is usually fabricated by using micro electrical-mechanical systems (MEMS) technology. Broadband wavelength tunability has already been demonstrated using this technique, and mainly for MEMS-VCSELs operating at wavelengths ranging from 850 nm [7] to 1550 nm [8]. These demonstrations have been both performed with optically [9], [10] and electrically pumped devices [2]–[8]. More recently, a MEMS structure based on a robust design has been also investigated [11]. However, for all these MEMS-VCSELs, weaknesses can be raised concerning the linewidth and stability of the emitted wavelength [12], [13] and there may be advantages in terms of lifetime, stability, and production cost by eliminating the free-standing element necessary in MEMS-tunable VCSELs.

A promising alternative to this MEMS approach is the use of liquid crystals (LC) which can provide a large refractive index tuning with a moderate driving voltage and very low power consumption. Several demonstrations have been conducted in the past to integrate LC within compact photonic devices such as ring resonators [14], photodiodes [15] or VCSELs [16]. However, there is only one demonstration reporting the use of LC inside a VCSEL cavity in order to tune its wavelength [17]. In this pioneering work, a macro-sized LC cell with unperfected thickness control led unfortunately to lasing operation in a pulsed regime only. More recently, simulations results have been published on a 1.55 μm-VCSEL designed with nematic LC enclosed within the VCSEL cavity, showing that a tuning range of 68 nm might be expected [18].

In this paper, we report for the first time CW operation at room temperature (RT) of a tunable VCSEL emitting at 1550 nm integrating a LC microcell monolithically fabricated on an InP-based half-cavity VCSEL. The design and fabrication steps are detailed. Laser characteristics are also presented, discussed and compared to thermo-optical simulations.

II. Design and Technology

Our tunable device consists of a micro-sized LC cell monolithically integrated above an InP-based half-VCSEL. For this first realization of a CW LC-VCSEL operating at RT, the semiconductor part of the cavity has been designed for optical pumping to simplify the fabrication process as much

Manuscript received December 23, 2019; revised February 10, 2020; accepted February 14, 2020. This work was supported in part by the Direction Générale de l'Armement (DGA) and in part by the French National Research Agency (ANR) under Grant ANR-14-ASTR-0007 HYPOCAMP and Grant ANR-15-CE19-0012 DOCT VCSEL. *(Corresponding author: C. Levallois.)*

B. Boisnard, T. Camps, B. Sadani, and V. Bardinal are with ~~Université~~ Toulouse, CNRS, LAAS, F-31400 Toulouse, France (e-mail: bardinal@laas.fr).

C. Levallois, C. Paranthoen, S. Pes, K. Tavernier, and M. Alouini are with ~~Université~~ Rennes, INSA Rennes, CNRS, Institut FOTON – UMR 6082, F-35000 Rennes, France (e-mail: christophe.Levallois@insa-rennes.fr).

S. Bouchoule is with C2N (Centre for Nanoscience and nanotechnology), CNRS, Université Paris-Sud, 91360 Marcoussis, France (e-mail: sophie.bouchoule@c2n.upsaclay.fr).

L. Dupont is with IMT Atlantique, Optics Department, 29200 Plouzané, France (e-mail: laurent.dupont@imt-atlantique.fr).

P. Debernardi is with Consiglio Nazionale delle Ricerche (CNR), IEIIT, 10129 Torino, Italy (e-mail: pierluigi.debernardi@ieiit.cnr.it).

Color versions of one or more of the figures in this letter are available online at http://ieeexplore.ieee.org.

Digital Object Identifier 10.1109/LPT.2020.2975076

IEEE Proof

1041-1135 © 2020 IEEE. Personal use is permitted, but republication/redistribution requires IEEE permission.
See https://www.ieee.org/publications/rights/index.html for more information.

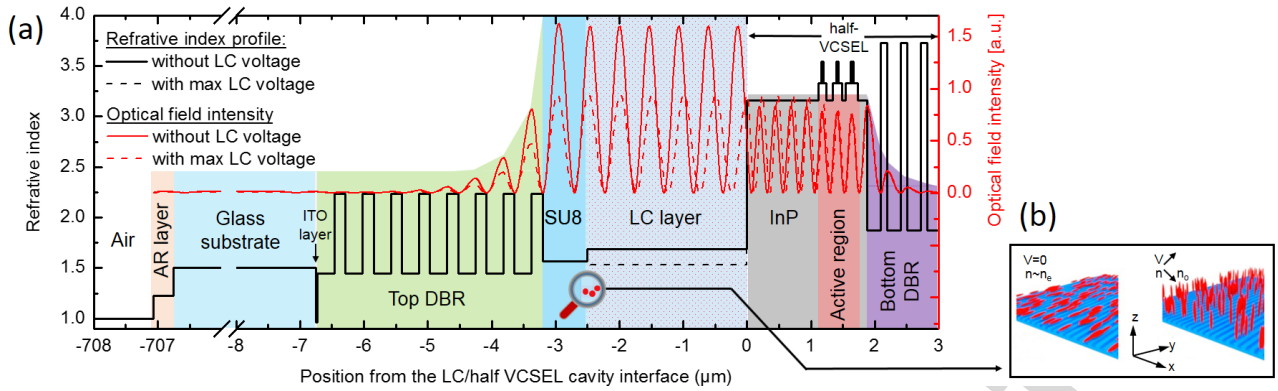

Fig. 1. (a) LC-VCSEL structure and internal optical field intensity for resonant modes related to the extraordinary index for two different voltages applied on the LC layer. (b) Enlarged schematic view of the subwavelength gratings printed on the SU8 layer for the LC alignment and reorientation of the LC molecules when AC voltage applied on the LC microcell is maximum.

as possible. The active region consists of 9 strained InGaAsP quantum wells (QWs) grown by gas source molecular beam epitaxy on an InP(001) substrate. These QWs, emitting at 1.55 μm, are distributed over three optical standing wave anti-node positions within the cavity. The bottom mirror is a 5×(SiN_x/aSi) periods DBR completed by a gold layer deposited by sputtering to reach a theoretical reflectivity from the inner cavity of 99.7%. This stack of layers is transferred onto a Si substrate by a polymer bonding using a 3 μm thick BCB layer. Then the InP substrate is removed by mechanical thinning and chemical etching to obtain the half-VCSEL (see Fig. 1(a) - right part).

The technological process then continues with the collective fabrication of LC microcells monolithically integrated onto the half-VCSEL surface derived from a method based on dry thick resist films [19]. First, a thick UV negative photoresist (MicroChem PermiNex 2000) is spin-coated on the sample and exposed through a mask to define squared areas, which will be filled by LC in the final processing steps. Those microcells are then covered by a top DBR with a theoretical reflectivity of 99.5%, consisting of 8 (SiO_2/TiO_2) periods deposited on a glass substrate, previously coated with a 23 nm thick ITO electrode to apply the voltage on the LC microcells. The second electrode connected to the ground corresponds to the gold layer deposited on top of the SiN_x/aSi mirror. The upper part of the device, covered by an antireflection layer at 1.55 μm, is then laminated to the top surface of the half-VCSEL at a low temperature (150°C). Prior to this step, the top mirror surface is prepared for further LC molecules alignment. This alignment is obtained through a planar anchoring on a sub-wavelength grating printed on a 600 nm thick SU8 layer before lamination. Reference [19] provides details about this part of the process. The sub-wavelength grating is patterned by a well-controlled nanoimprint process to define a period of 780 nm, a duty cycle of 50:50, and a depth in the range of [70-80 nm]. This grating, schematically depicted as a blue layer in Fig. 1(b), has been designed to allow an efficient orientation of the LC molecules during the microcells filling while limiting optical losses by diffraction at the wavelength of 1.55 μm.

The final step consists in filling the microcells under vacuum with a nematic LC similar to E7. This filling is achieved at a temperature higher than the nematic-isotropic transition (70 °C) thanks to lateral apertures previously defined in the PermiNex photoresist. All the layers and their associated refractive indices are represented in Fig. 1. The distribution of the stationary field inside the VCSEL cavity is also illustrated for both cases, without applied voltage and for maximum applied voltage, i.e. when all the LC molecules are reoriented. As illustrated Fig. 1(b), without voltage, the average orientation of the LC molecules (i.e. the director) is parallel to the surface, and the refractive index is maximum (close to the extraordinary index, n_e). As the applied voltage increases, the director is reoriented and the refractive index decreases towards n_0 (the ordinary index) leading to a blue shift of the resonant wavelength. To avoid polarization bistability in the VCSEL, special attention has been paid to the cavity design. In particular, the LC thickness has been adjusted in order to reject the resonant modes related to n_0 (being not affected by the applied voltage) far from the maximum gain of the QWs, while keeping a resonant mode related to n_e centered in the spectral window emitted by the QWs. The resonant mode with a linear polarization parallel (or perpendicular) to the director will be referred to as “EM for extraordinary mode” (or “OM for ordinary mode”) in the following.

III. Results and Discussion

After the fabrication stage, the tunable VCSEL has been placed on a Peltier thermoelectric cooler and characterized under optical pumping using a CW 980 nm semiconductor fibered laser diode focused on a 15 μm diameter spot ($1/e^2$ waist size). Fig. 2 shows the VCSEL output power as a function of the absorbed pump power, measured for different voltages applied on the LC microcells. As shown in Fig. 2, the tunable VCSEL exhibits CW operation at 17°C with a threshold power at around 6.5 mW. This threshold is not strongly dependent on the applied voltage and corresponds to a threshold power density of a few kW · cm^{-2}, very close to the ones previously reported for equivalent VCSELs incorporating no LC [20]. Thus, as expected and demonstrated in previous works [15], [19], the presence of the LC leads to negligible additional losses, even in such highly sensitive VCSEL structure. However, this LC layer has a significant impact on the stability of the VCSEL emission. As illustrated

IEEE Proof

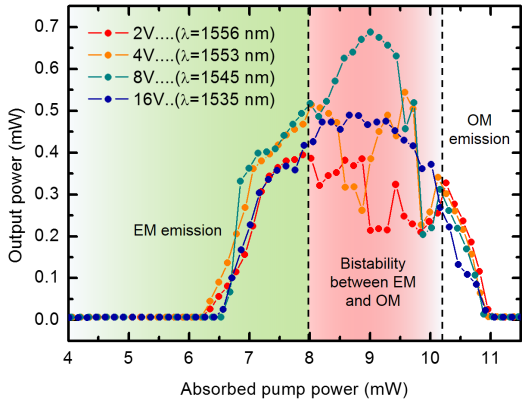

Fig. 2. Output power emitted as a function of the absorbed pump power for different AC voltages (20 kHz) applied on the LC microcells. Also shown are the different working areas where the VCSEL operates according to the extraordinary mode (EM), the ordinary mode (OM), or in a bi-stability regime between both modes.

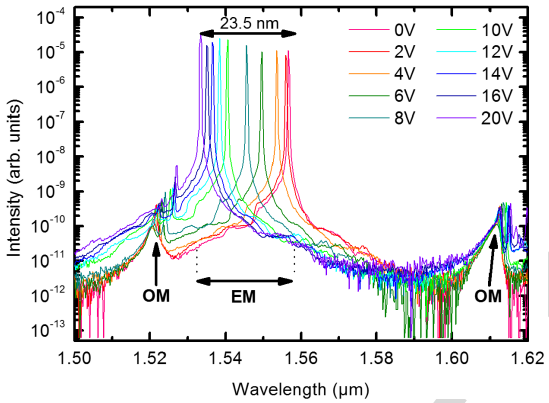

Fig. 3. VCSEL output spectra (290K, CW) measured for different AC voltages (20 kHz) applied on the LC and at a constant pump power set just below the unstable operation area (7.8 mW). The arrows give the spectral positions of the tunable lasing EM and the non-lasing OM corresponding respectively to the extraordinary (n_e) and ordinary (n_0) refractive indices of the LC.

in Fig. 2, the laser emission occurs in the EM near the threshold, but switches to the OM for high pump powers. For intermediate powers, a bistable emission is observed between OM and EM leading to strong fluctuations in the output powers, which are very dependent on the pump power itself but also on the LC voltage.

Consequently, the tuning range has been measured for a pump power of 7.8 mW, at the upper limit of the stability area, for a laser emission exclusively in EM. With such a pump power, the output power ranges between 0.35 mW and 0.5 mW for applied voltages in the 0 V-16 V range. Fig. 3 represents lasing spectra recorded for LC voltages ranging from 0 V to 20 V. Without any applied voltage on the LC, the lasing wavelength is centered at 1556.5 nm, and is continuously blue-shifted down to 1533.1 nm when the voltage is increased to 20 V, leading to an available tuning range of 23.5 nm.

This blue-shift of the lasing wavelength related to the EM is consistent with the fact that n_e decreases with the applied electric field on the LC layer. The wavelength shift starts at 2 V with a tuning efficiency close to 2 nm/V between 2 V and 10 V, which decreases to 0.7 nm/V above 10 V when most LC molecules have been reoriented along the applied electric field. For higher voltages than 20 V the EM does not shift anymore which means that n_e has decreased but never reaches the n_0 value. Also, as indicated in Fig. 3, two peaks identified as being OM are located at 1521.6 nm and 1612.3 nm. These peaks are red-shifted by 5.4 nm and 3.2 nm respectively when the voltage is increased, the red-shifting being even more pronounced for high voltages when the OM and EM become closer. There are clear indications that this unexpected OM wavelength shift might be related to a tuning-dependent temperature rise in the device. For pulsed pumping, this dependence disappears and it is well known that temperature has an impact on both EM and OM indices [21]. The thermal issue is always an important factor in VCSEL operation, but for this first proof of concept, the thermal resistance has not been optimized. Indeed, the thick InP layer (1.15 μm) which is transparent at the pump wavelength does not offer a strong thermal insulation between LC and the heated active region of the VCSEL. Furthermore, the employed bonding method to attach the III-V active region onto a Si substrate by using BCB polymer is not the best approach to minimize the thermal resistance of the VCSEL ($R_{th} \sim 3000$ K/W) [20].

In the following, we try to investigate more in details the tuning features of our device by comparing the experimental wavelength dependence with the computed ones. The simulations are based on a modified 1D-TMM (transfer matrix method) code, where the LC anchoring grating is taken into account using a Rigorous Couple Wave Analysis (RCWA). RCWA provides the transmission matrix of the grating, when the 1D-TMM analytical approach is used for the rest of the layers. The 1D-TMM code is applied for n_o and n_e providing the resonant wavelengths, QW material gain, and the corresponding standing wave profile for each resonant wavelength (see Fig. 1). The threshold gains are computed mainly to check that OM experiences a higher threshold, and thus to ensure that EM is the lasing mode as requested, which is confirmed by Fig. 4(c).

The quantitative investigation can be performed only on the mode lines and their dependence with the tuning voltage. Therefore these quantities have been extracted from Fig. 3 and reported in Fig. 4(a). Because of the nearly linear relation between LC indices and emission wavelengths, a similar dependence of the index vs. tuning voltage is assumed. This is fairly well approximated by the phenomenological dependence:

$$n_i = n_{i0} + \left[1 + \cos\frac{\pi V}{V_m}\right].\frac{dn_i}{2}$$

where, i is either e or o, and V and V_m are the tuning voltage and the maximum voltage respectively. The four index parameters are determined in such a way that the best fit of the modal lines is obtained. This yields: $n_e = 1.68$, $dn_e = -0.13$, $n_o = 1.5$, $dn_o = +0.02$. The corresponding curves are shown in Fig. 4(b) and it is to be noted that a very similar dependence is proposed in [22]. The lower bound of the extraordinary index does not reach its ideal value (n_o), which can be attributed to a portion of inactive LC molecules that do not react to the voltage.

IEEE Proof

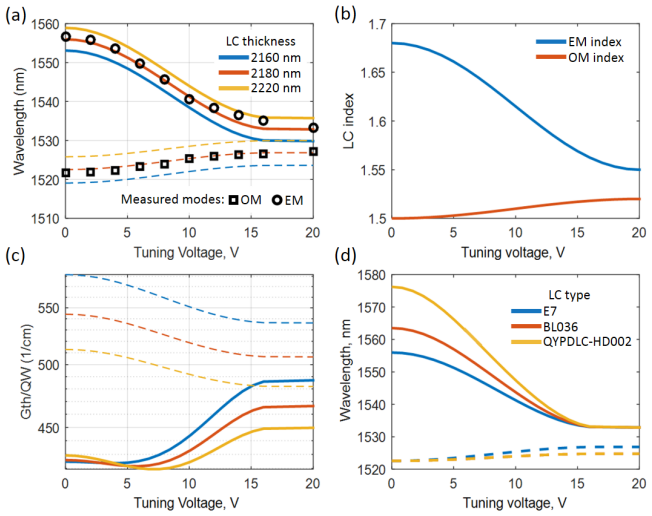

Fig. 4. (a) Computed emission wavelength of the EM/OM (continuous/dashed lines) vs. voltage for three different LC microcell thicknesses (see legend). Open squares and circles refer to the experimental results from Fig. 2. (b) Phenomenological LC index dependence on applied voltage. (c) Threshold gain corresponding to tuning curves of Fig. 4(a). (d) Similar to (a), but with different LC types (see legend).

The fine tuning of the emission wavelength is achieved by varying the SU8 thickness and the LC microcell thickness within the following tolerance ranges: 600±150 nm and 2300±150 nm. Agreement is obtained for a thickness value of 700 nm for the SU8 layer, and 2180 nm for the microcell. In Fig. 4(a), the effect of finely varying the latter thickness is shown.

Thus, satisfactory matching between experiment and simulation is found, pointing to an efficiency degradation in comparison with the nominal range of 1.72-1.52 expected for our nematic LC. This reduction in the LC birefringence, and thus in the wavelength tuning, is mainly attributed to its thermal dependence leading to a collapse of the LC birefringence around 60°C. Accordingly, the use of a nematic QYPDL-HD002 LC is expected to provide a higher tuning range, close to 45 nm as illustrated in Fig. 4(d).

IV. Conclusion

A 1.55 μm InP-VCSEL with CW operation at RT and 23.5 nm wavelength tunability has been designed, fabricated and characterized. This device combines InP-based materials with LC microcells collectively fabricated and integrated on the surface of a half-cavity VCSEL. The maximum driving voltage applied to the LC is 20 V without any apparent current leakage, leading to low power consumption for the wavelength control of the device. In addition, simulations based on the experimental results have been conducted to identify the discrepancy between expected and observed spectral behavior. It turns out that the appearing reduction of LC birefringence is induced by thermal conduction between the active medium and the LC microcell. Finally, by using LC with a better thermal tolerance larger tuning ranges are expected. Further work includes investigation of the dynamical behavior of wavelength tuning. Indeed, typical response time of such LC being in the millisecond range, a frequency chirp of 4 THz/ms could be reached for coherent Lidar applications.

Acknowledgment

The authors would like to thank RENATECH/ RENATECH+ (the French national network of facilities for micronanotechnology) with LAAS-CNRS, C2N-CNRS/ UPSUD, and NanoRennes for technological support.

References

[1] J. Skidmore, "Semiconductor Lasers for 3-D Sensing," *Opt. Photon. News*, vol. 30, pp. 26–33, Feb-2019.

[2] B. Kogel *et al.*, "Simultaneous spectroscopy of NH_3 and CO using a > 50 nm continuously tunable MEMS-VCSEL," *IEEE Sensors J.*, vol. 7, no. 11, pp. 1483–1489, Nov. 2007.

[3] B. Potsaid, V. Jayaraman, J. G. Fujimoto, J. Jiang, P. J. S. Heim, and A. E. Cable, "MEMS tunable VCSEL light source for ultrahigh speed 60 kHz–1MHz axial scan rate and long range centimeter class OCT imaging," in *Proc. 16th Opt. Coherence Tomogr. Coherence Domain Opt. Methods Biomed.*, Feb. 2012, p. 82130.

[4] D. D. John *et al.*, "Wideband electrically pumped 1050-nm MEMS-tunable VCSEL for ophthalmic imaging," *J. Lightw. Technol.*, vol. 33, no. 16, pp. 3461–3468, Aug. 15, 2015.

[5] C. F. R. Mateus and C. L. Barbosa, "Harsh environment temperature and strain sensor using tunable VCSEL and multiple fiber Bragg gratings," in *IEEE MTT-S Int. Microw. Symp. Dig.*, 2007, pp. 496–498.

[6] V. J. Kitsmiller, M. M. Dummer, K. Johnson, G. D. Cole, and T. D. O'Sullivan, "Frequency domain diffuse optical spectroscopy with a near-infrared tunable vertical cavity surface emitting laser," *Opt. Express*, vol. 26, no. 16, p. 21033, Jul. 2018.

[7] D. D. John *et al.*, "Single-mode and high-speed 850 nm MEMS-VCSEL," in *Proc. Lasers Congr. (ASSL, LSC, LAC)*, Boston, MA, USA, 2016, pp. 1–4, Paper ATh5A.2.

[8] C. Gierl *et al.*, "Surface micromachined tunable 155 μm-VCSEL with 102 nm continuous single-mode tuning," *Opt. Express*, vol. 19, no. 18, p. 17336, Aug. 2011.

[9] V. Jayaraman, G. D. Cole, M. Robertson, A. Uddin, and A. Cable, "High-sweep-rate 1310 nm MEMS-VCSEL with 150 nm continuous tuning range," *Electron. Lett.*, vol. 48, no. 14, p. 867, 2012.

[10] V. Jayaraman *et al.*, "Rapidly swept, ultra-widely-tunable 1060 nm MEMS-VCSELs," *Electron. Lett.*, vol. 48, no. 21, p. 1331, 2012.

[11] H. K. Sahoo *et al.*, "Tunable MEMS VCSEL on silicon substrate," *IEEE J. Sel. Topics Quantum Electron.*, vol. 25, no. 6, pp. 1–7, Nov. 2019.

[12] H. Halbritter, C. Sydlo, B. Kogel, F. Riemenschneider, H. L. Hartnagel, and P. Meissner, "Impact of micromechanics on the linewidth and chirp performance of MEMS-VCSELs," *IEEE J. Sel. Topics Quantum Electron.*, vol. 13, no. 2, pp. 367–373, Apr. 2007.

[13] S. Paul *et al.*, "Far-field, linewidth and thermal characteristics of a high-speed 1550-nm MEMS tunable VCSEL," *Opt. Express*, vol. 24, no. 12, p. 13142, Jun. 2016.

[14] W. De Cort, J. Beeckman, T. Claes, K. Neyts, and R. Baets, "Wide tuning of silicon-on-insulator ring resonators with a liquid crystal cladding," *Opt. Lett.*, vol. 36, no. 19, pp. 3876–3878, Sep. 2011.

[15] C. Levallois *et al.*, "Liquid crystal-based tunable photodetector operating in the telecom C-band," *Opt. Express*, vol. 26, no. 20, Sep. 2018, Art. no. 25952.

[16] Y. Xie, J. Beeckman, W. Woestenborghs, K. Panajotov, and K. Neyts, "VCSEL with photo-aligned liquid crystal overlay," *IEEE Photon. Technol. Lett.*, vol. 24, no. 17, pp. 1509–1512, Sep. 2012.

[17] O. Castany, L. Dupont, A. Shuaib, J. P. Gauthier, C. Levallois, and C. Paranthoën, "Tunable semiconductor vertical-cavity surface-emitting laser with an intracavity liquid crystal layer," *Appl. Phys. Lett.*, vol. 98, no. 16, Apr. 2011, Art. no. 161105.

[18] L. Frasunkiewicz, T. Czyszanowski, H. Thienpont, and K. Panajotov, "Electrically tunable VCSEL with intra-cavity liquid crystal: Design, optimization, and analysis of polarization- and mode-stability," *Opt. Commun.*, vol. 427, pp. 271–277, Nov. 2018.

[19] B. Sadani *et al.*, "Liquid-crystal alignment by a nanoimprinted grating for wafer-scale fabrication of tunable devices," *IEEE Photon. Technol. Lett.*, vol. 30, no. 15, pp. 1388–1391, Aug. 1, 2018.

[20] F. Taleb *et al.*, "Enhancement of VCSEL performances using localized copper bonding through silicon vias," *IEEE Photon. Technol. Lett.*, vol. 29, no. 13, pp. 1105–1108, Jul. 1, 2017.

[21] J. Li, S.-T. Wu, S. Brugioni, R. Meucci, and S. Faetti, "Infrared refractive indices of liquid crystals," *J. Appl. Phys.*, vol. 97, pp. 073501-1–073501-5, Mar. 2005.

[22] C. Belmonte *et al.*, "Optimization of electrically tunable VCSEL with intracavity nematic liquid crystal," *Opt. Express*, vol. 23, no. 12, p. 15706, Jun. 2015.

IEEE Proof

CW Operation of a Tunable 1550-nm VCSEL Integrating Liquid-Crystal Microcells

B. Boisnard, C. Levallois, C. Paranthoen, S. Pes, T. Camps, B. Sadani, K. Tavernier, S. Bouchoule, L. Dupont, M. Alouini, P. Debernardi, and V. Bardinal

***Abstract*— An InP-based Vertical-Cavity Surface-Emitting Laser (VCSEL) with a liquid crystal (LC) microcell monolithically integrated on its surface for spectral tuning is investigated. Unlike tunable VCSELs integrating a movable membrane, here the physical length of the cavity remains unchanged and only the voltage applied on the LC ensures a refractive index modification for a particular polarization emitted by the VCSEL. This tunable VCSEL operates in CW at room temperature and exhibits more than 23 nm wavelength tuning around 1.55 μm at a maximum applied voltage of 20 V. The measured laser threshold around 6.5 mW is still comparable to VCSEL without LC microcell, a clear indication that the optical losses related the LC are very low. On the other hand, for this first optically pumped device, the lasing characteristics suggest that the LC birefringence is lower than expected. To assess this hypothesis, thermo-optical simulations have been conducted.**

***Index Terms*— Vertical-cavity surface-emitting lasers, liquid crystal devices, semiconductor lasers.**

I. Introduction

VERTICAL-CAVITY Surface-Emitting Lasers (VCSELs) are key optical sources for optical communications, and more recently for applications like autofocus imaging or facial recognition on smartphones [1]. Their well-known advantages related to longitudinal single-mode emission, circular beam shape with a low divergence, low-power consumption, and an easy 2D integration for mass production are very attractive for such applications. However, for a wider range of applications, including gas sensing [2], Optical Coherence Tomography (OCT) [3], [4], Fiber Bragg Grating (FBG) sensing [5] and optical spectroscopy [6], wavelength tunability is required. In this case, the large free spectral range related to the VCSEL microcavity becomes interesting to obtain a wide spectral tunability without mode hopping. To realize such tunable VCSEL, it is then required to change the optical length of the cavity. The most used technique is based on the variation of the physical length of the optical resonator. This is typically achieved by thermal or electrostatic actuation of a suspended membrane acting as a movable end mirror for the cavity, which is usually fabricated by using micro electrical-mechanical systems (MEMS) technology. Broadband wavelength tunability has already been demonstrated using this technique, and mainly for MEMS-VCSELs operating at wavelengths ranging from 850 nm [7] to 1550 nm [8]. These demonstrations have been both performed with optically [9], [10] and electrically pumped devices [2]–[8]. More recently, a MEMS structure based on a robust design has been also investigated [11]. However, for all these MEMS-VCSELs, weaknesses can be raised concerning the linewidth and stability of the emitted wavelength [12], [13] and there may be advantages in terms of lifetime, stability, and production cost by eliminating the free-standing element necessary in MEMS-tunable VCSELs.

A promising alternative to this MEMS approach is the use of liquid crystals (LC) which can provide a large refractive index tuning with a moderate driving voltage and very low power consumption. Several demonstrations have been conducted in the past to integrate LC within compact photonic devices such as ring resonators [14], photodiodes [15] or VCSELs [16]. However, there is only one demonstration reporting the use of LC inside a VCSEL cavity in order to tune its wavelength [17]. In this pioneering work, a macro-sized LC cell with unperfected thickness control led unfortunately to lasing operation in a pulsed regime only. More recently, simulations results have been published on a 1.55 μm-VCSEL designed with nematic LC enclosed within the VCSEL cavity, showing that a tuning range of 68 nm might be expected [18].

In this paper, we report for the first time CW operation at room temperature (RT) of a tunable VCSEL emitting at 1550 nm integrating a LC microcell monolithically fabricated on an InP-based half-cavity VCSEL. The design and fabrication steps are detailed. Laser characteristics are also presented, discussed and compared to thermo-optical simulations.

II. Design and Technology

Our tunable device consists of a micro-sized LC cell monolithically integrated above an InP-based half-VCSEL. For this first realization of a CW LC-VCSEL operating at RT, the semiconductor part of the cavity has been designed for optical pumping to simplify the fabrication process as much

Manuscript received December 23, 2019; revised February 10, 2020; accepted February 14, 2020. This work was supported in part by the Direction Générale de l'Armement (DGA) and in part by the French National Research Agency (ANR) under Grant ANR-14-ASTR-0007 HYPOCAMP and Grant ANR-15-CE19-0012 DOCT VCSEL. *(Corresponding author: C. Levallois.)*

B. Boisnard, T. Camps, B. Sadani, and V. Bardinal are with Université Toulouse, CNRS, LAAS, F-31400 Toulouse, France (e-mail: bardinal@laas.fr).

C. Levallois, C. Paranthoen, S. Pes, K. Tavernier, and M. Alouini are with Université Rennes, INSA Rennes, CNRS, Institut FOTON – UMR 6082, F-35000 Rennes, France (e-mail: christophe.Levallois@insa-rennes.fr).

S. Bouchoule is with C2N (Centre for Nanoscience and nanotechnology), CNRS, Université Paris-Sud, 91360 Marcoussis, France (e-mail: sophie.bouchoule@c2n.upsaclay.fr).

L. Dupont is with IMT Atlantique, Optics Department, 29200 Plouzané, France (e-mail: laurent.dupont@imt-atlantique.fr).

P. Debernardi is with Consiglio Nazionale delle Ricerche (CNR), IEIIT, 10129 Torino, Italy (e-mail: pierluigi.debernardi@ieiit.cnr.it).

Color versions of one or more of the figures in this letter are available online at http://ieeexplore.ieee.org.

Digital Object Identifier 10.1109/LPT.2020.2975076

IEEE Proof

1041-1135 © 2020 IEEE. Personal use is permitted, but republication/redistribution requires IEEE permission.
See https://www.ieee.org/publications/rights/index.html for more information.

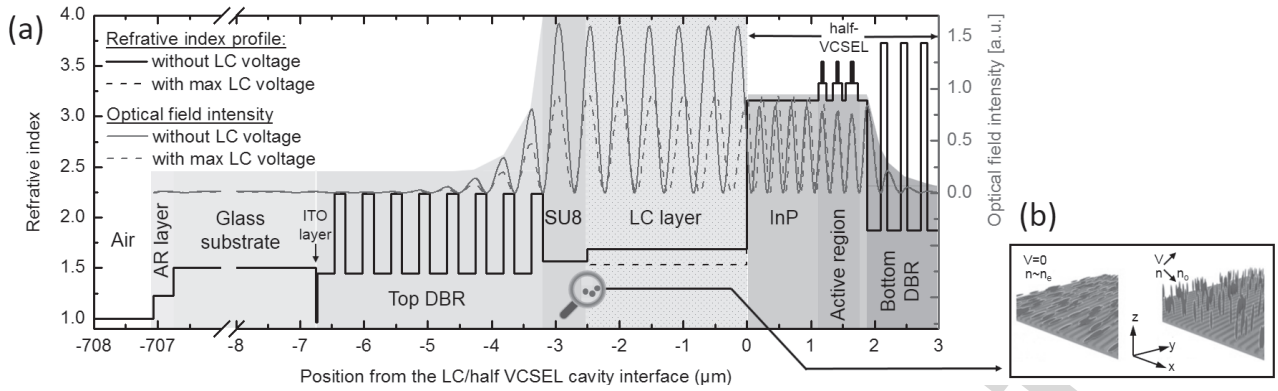

Fig. 1. (a) LC-VCSEL structure and internal optical field intensity for resonant modes related to the extraordinary index for two different voltages applied on the LC layer. (b) Enlarged schematic view of the subwavelength gratings printed on the SU8 layer for the LC alignment and reorientation of the LC molecules when AC voltage applied on the LC microcell is maximum.

as possible. The active region consists of 9 strained InGaAsP quantum wells (QWs) grown by gas source molecular beam epitaxy on an InP(001) substrate. These QWs, emitting at 1.55 μm, are distributed over three optical standing wave anti-node positions within the cavity. The bottom mirror is a 5×(SiN_x/aSi) periods DBR completed by a gold layer deposited by sputtering to reach a theoretical reflectivity from the inner cavity of 99.7%. This stack of layers is transferred onto a Si substrate by a polymer bonding using a 3 μm thick BCB layer. Then the InP substrate is removed by mechanical thinning and chemical etching to obtain the half-VCSEL (see Fig. 1(a) - right part).

The technological process then continues with the collective fabrication of LC microcells monolithically integrated onto the half-VCSEL surface derived from a method based on dry thick resist films [19]. First, a thick UV negative photoresist (MicroChem PermiNex 2000) is spin-coated on the sample and exposed through a mask to define squared areas, which will be filled by LC in the final processing steps. Those microcells are then covered by a top DBR with a theoretical reflectivity of 99.5%, consisting of 8 (SiO_2/TiO_2) periods deposited on a glass substrate, previously coated with a 23 nm thick ITO electrode to apply the voltage on the LC microcells. The second electrode connected to the ground corresponds to the gold layer deposited on top of the SiN_x/aSi mirror. The upper part of the device, covered by an antireflection layer at 1.55 μm, is then laminated to the top surface of the half-VCSEL at a low temperature (150°C). Prior to this step, the top mirror surface is prepared for further LC molecules alignment. This alignment is obtained through a planar anchoring on a sub-wavelength grating printed on a 600 nm thick SU8 layer before lamination. Reference [19] provides details about this part of the process. The sub-wavelength grating is patterned by a well-controlled nanoimprint process to define a period of 780 nm, a duty cycle of 50:50, and a depth in the range of [70-80 nm]. This grating, schematically depicted as a blue layer in Fig. 1(b), has been designed to allow an efficient orientation of the LC molecules during the microcells filling while limiting optical losses by diffraction at the wavelength of 1.55 μm.

The final step consists in filling the microcells under vacuum with a nematic LC similar to E7. This filling is achieved at a temperature higher than the nematic-isotropic transition (70 °C) thanks to lateral apertures previously defined in the PermiNex photoresist. All the layers and their associated refractive indices are represented in Fig. 1. The distribution of the stationary field inside the VCSEL cavity is also illustrated for both cases, without applied voltage and for maximum applied voltage, i.e. when all the LC molecules are reoriented. As illustrated Fig. 1(b), without voltage, the average orientation of the LC molecules (i.e. the director) is parallel to the surface, and the refractive index is maximum (close to the extraordinary index, n_e). As the applied voltage increases, the director is reoriented and the refractive index decreases towards n_0 (the ordinary index) leading to a blue shift of the resonant wavelength. To avoid polarization bistability in the VCSEL, special attention has been paid to the cavity design. In particular, the LC thickness has been adjusted in order to reject the resonant modes related to n_0 (being not affected by the applied voltage) far from the maximum gain of the QWs, while keeping a resonant mode related to n_e centered in the spectral window emitted by the QWs. The resonant mode with a linear polarization parallel (or perpendicular) to the director will be referred to as "EM for extraordinary mode" (or "OM for ordinary mode") in the following.

III. Results and Discussion

After the fabrication stage, the tunable VCSEL has been placed on a Peltier thermoelectric cooler and characterized under optical pumping using a CW 980 nm semiconductor fibered laser diode focused on a 15 μm diameter spot ($1/e^2$ waist size). Fig. 2 shows the VCSEL output power as a function of the absorbed pump power, measured for different voltages applied on the LC microcells. As shown in Fig. 2, the tunable VCSEL exhibits CW operation at 17°C with a threshold power at around 6.5 mW. This threshold is not strongly dependent on the applied voltage and corresponds to a threshold power density of a few kW · cm^{-2}, very close to the ones previously reported for equivalent VCSELs incorporating no LC [20]. Thus, as expected and demonstrated in previous works [15], [19], the presence of the LC leads to negligible additional losses, even in such highly sensitive VCSEL structure. However, this LC layer has a significant impact on the stability of the VCSEL emission. As illustrated

IEEE Proof

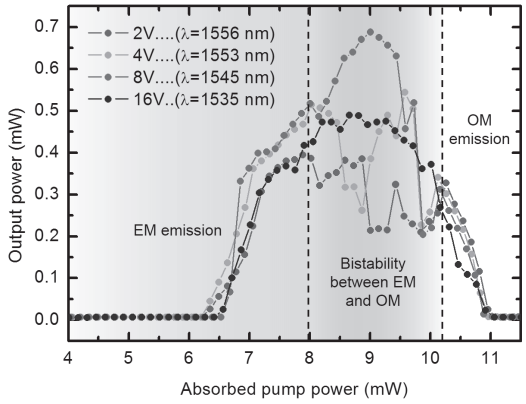

Fig. 2. Output power emitted as a function of the absorbed pump power for different AC voltages (20 kHz) applied on the LC microcells. Also shown are the different working areas where the VCSEL operates according to the extraordinary mode (EM), the ordinary mode (OM), or in a bi-stability regime between both modes.

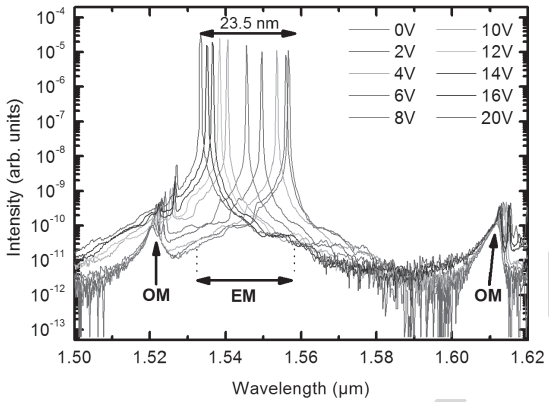

Fig. 3. VCSEL output spectra (290K, CW) measured for different AC voltages (20 kHz) applied on the LC and at a constant pump power set just below the unstable operation area (7.8 mW). The arrows give the spectral positions of the tunable lasing EM and the non-lasing OM corresponding respectively to the extraordinary (n_e) and ordinary (n_0) refractive indices of the LC.

in Fig. 2, the laser emission occurs in the EM near the threshold, but switches to the OM for high pump powers. For intermediate powers, a bistable emission is observed between OM and EM leading to strong fluctuations in the output powers, which are very dependent on the pump power itself but also on the LC voltage.

Consequently, the tuning range has been measured for a pump power of 7.8 mW, at the upper limit of the stability area, for a laser emission exclusively in EM. With such a pump power, the output power ranges between 0.35 mW and 0.5 mW for applied voltages in the 0 V-16 V range. Fig. 3 represents lasing spectra recorded for LC voltages ranging from 0 V to 20 V. Without any applied voltage on the LC, the lasing wavelength is centered at 1556.5 nm, and is continuously blue-shifted down to 1533.1 nm when the voltage is increased to 20 V, leading to an available tuning range of 23.5 nm.

This blue-shift of the lasing wavelength related to the EM is consistent with the fact that n_e decreases with the applied electric field on the LC layer. The wavelength shift starts at 2 V with a tuning efficiency close to 2 nm/V between 2 V and 10 V, which decreases to 0.7 nm/V above 10 V when most LC molecules have been reoriented along the applied electric field. For higher voltages than 20 V the EM does not shift anymore which means that n_e has decreased but never reaches the n_0 value. Also, as indicated in Fig. 3, two peaks identified as being OM are located at 1521.6 nm and 1612.3 nm. These peaks are red-shifted by 5.4 nm and 3.2 nm respectively when the voltage is increased, the red-shifting being even more pronounced for high voltages when the OM and EM become closer. There are clear indications that this unexpected OM wavelength shift might be related to a tuning-dependent temperature rise in the device. For pulsed pumping, this dependence disappears and it is well known that temperature has an impact on both EM and OM indices [21]. The thermal issue is always an important factor in VCSEL operation, but for this first proof of concept, the thermal resistance has not been optimized. Indeed, the thick InP layer (1.15 μm) which is transparent at the pump wavelength does not offer a strong thermal insulation between LC and the heated active region of the VCSEL. Furthermore, the employed bonding method to attach the III-V active region onto a Si substrate by using BCB polymer is not the best approach to minimize the thermal resistance of the VCSEL ($R_{th} \sim 3000$ K/W) [20].

In the following, we try to investigate more in details the tuning features of our device by comparing the experimental wavelength dependence with the computed ones. The simulations are based on a modified 1D-TMM (transfer matrix method) code, where the LC anchoring grating is taken into account using a Rigorous Couple Wave Analysis (RCWA). RCWA provides the transmission matrix of the grating, when the 1D-TMM analytical approach is used for the rest of the layers. The 1D-TMM code is applied for n_o and n_e providing the resonant wavelengths, QW material gain, and the corresponding standing wave profile for each resonant wavelength (see Fig. 1). The threshold gains are computed mainly to check that OM experiences a higher threshold, and thus to ensure that EM is the lasing mode as requested, which is confirmed by Fig. 4(c).

The quantitative investigation can be performed only on the mode lines and their dependence with the tuning voltage. Therefore these quantities have been extracted from Fig. 3 and reported in Fig. 4(a). Because of the nearly linear relation between LC indices and emission wavelengths, a similar dependence of the index vs. tuning voltage is assumed. This is fairly well approximated by the phenomenological dependence:

$$n_i = n_{i0} + \left[1 + \cos\frac{\pi V}{V_m}\right].\frac{dn_i}{2}$$

where, i is either e or o, and V and V_m are the tuning voltage and the maximum voltage respectively. The four index parameters are determined in such a way that the best fit of the modal lines is obtained. This yields: $n_e = 1.68$, $dn_e = -0.13$, $n_o = 1.5$, $dn_o = +0.02$. The corresponding curves are shown in Fig. 4(b) and it is to be noted that a very similar dependence is proposed in [22]. The lower bound of the extraordinary index does not reach its ideal value (n_o), which can be attributed to a portion of inactive LC molecules that do not react to the voltage.

IEEE Proof

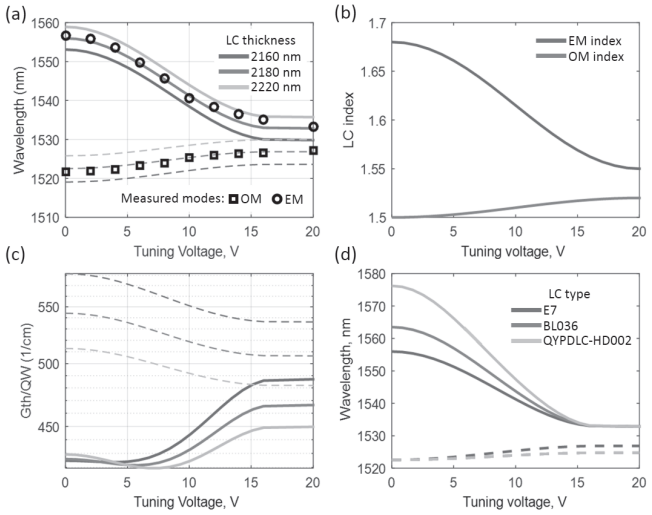

Fig. 4. (a) Computed emission wavelength of the EM/OM (continuous/dashed lines) vs. voltage for three different LC microcell thicknesses (see legend). Open squares and circles refer to the experimental results from Fig. 2. (b) Phenomenological LC index dependence on applied voltage. (c) Threshold gain corresponding to tuning curves of Fig. 4(a). (d) Similar to (a), but with different LC types (see legend).

The fine tuning of the emission wavelength is achieved by varying the SU8 thickness and the LC microcell thickness within the following tolerance ranges: 600±150 nm and 2300±150 nm. Agreement is obtained for a thickness value of 700 nm for the SU8 layer, and 2180 nm for the microcell. In Fig. 4(a), the effect of finely varying the latter thickness is shown.

Thus, satisfactory matching between experiment and simulation is found, pointing to an efficiency degradation in comparison with the nominal range of 1.72-1.52 expected for our nematic LC. This reduction in the LC birefringence, and thus in the wavelength tuning, is mainly attributed to its thermal dependence leading to a collapse of the LC birefringence around 60°C. Accordingly, the use of a nematic QYPDL-HD002 LC is expected to provide a higher tuning range, close to 45 nm as illustrated in Fig. 4(d).

IV. Conclusion

A 1.55 μm InP-VCSEL with CW operation at RT and 23.5 nm wavelength tunability has been designed, fabricated and characterized. This device combines InP-based materials with LC microcells collectively fabricated and integrated on the surface of a half-cavity VCSEL. The maximum driving voltage applied to the LC is 20 V without any apparent current leakage, leading to low power consumption for the wavelength control of the device. In addition, simulations based on the experimental results have been conducted to identify the discrepancy between expected and observed spectral behavior. It turns out that the appearing reduction of LC birefringence is induced by thermal conduction between the active medium and the LC microcell. Finally, by using LC with a better thermal tolerance larger tuning ranges are expected. Further work includes investigation of the dynamical behavior of wavelength tuning. Indeed, typical response time of such LC being in the millisecond range, a frequency chirp of 4 THz/ms could be reached for coherent Lidar applications.

Acknowledgment

The authors would like to thank RENATECH/ RENATECH+ (the French national network of facilities for micronanotechnology) with LAAS-CNRS, C2N-CNRS/ UPSUD, and NanoRennes for technological support.

References

[1] J. Skidmore, "Semiconductor Lasers for 3-D Sensing," *Opt. Photon. News*, vol. 30, pp. 26–33, Feb-2019.

[2] B. Kogel *et al.*, "Simultaneous spectroscopy of NH_3 and CO using a > 50 nm continuously tunable MEMS-VCSEL," *IEEE Sensors J.*, vol. 7, no. 11, pp. 1483–1489, Nov. 2007.

[3] B. Potsaid, V. Jayaraman, J. G. Fujimoto, J. Jiang, P. J. S. Heim, and A. E. Cable, "MEMS tunable VCSEL light source for ultrahigh speed 60 kHz–1MHz axial scan rate and long range centimeter class OCT imaging," in *Proc. 16th Opt. Coherence Tomogr. Coherence Domain Opt. Methods Biomed.*, Feb. 2012, p. 82130.

[4] D. D. John *et al.*, "Wideband electrically pumped 1050-nm MEMS-tunable VCSEL for ophthalmic imaging," *J. Lightw. Technol.*, vol. 33, no. 16, pp. 3461–3468, Aug. 15, 2015.

[5] C. F. R. Mateus and C. L. Barbosa, "Harsh environment temperature and strain sensor using tunable VCSEL and multiple fiber Bragg gratings," in *IEEE MTT-S Int. Microw. Symp. Dig.*, 2007, pp. 496–498.

[6] V. J. Kitsmiller, M. M. Dummer, K. Johnson, G. D. Cole, and T. D. O'Sullivan, "Frequency domain diffuse optical spectroscopy with a near-infrared tunable vertical cavity surface emitting laser," *Opt. Express*, vol. 26, no. 16, p. 21033, Jul. 2018.

[7] D. D. John *et al.*, "Single-mode and high-speed 850 nm MEMS-VCSEL," in *Proc. Lasers Congr. (ASSL, LSC, LAC)*, Boston, MA, USA, 2016, pp. 1–4, Paper ATh5A.2.

[8] C. Gierl *et al.*, "Surface micromachined tunable 155 μm-VCSEL with 102 nm continuous single-mode tuning," *Opt. Express*, vol. 19, no. 18, p. 17336, Aug. 2011.

[9] V. Jayaraman, G. D. Cole, M. Robertson, A. Uddin, and A. Cable, "High-sweep-rate 1310 nm MEMS-VCSEL with 150 nm continuous tuning range," *Electron. Lett.*, vol. 48, no. 14, p. 867, 2012.

[10] V. Jayaraman *et al.*, "Rapidly swept, ultra-widely-tunable 1060 nm MEMS-VCSELs," *Electron. Lett.*, vol. 48, no. 21, p. 1331, 2012.

[11] H. K. Sahoo *et al.*, "Tunable MEMS VCSEL on silicon substrate," *IEEE J. Sel. Topics Quantum Electron.*, vol. 25, no. 6, pp. 1–7, Nov. 2019.

[12] H. Halbritter, C. Sydlo, B. Kogel, F. Riemenschneider, H. L. Hartnagel, and P. Meissner, "Impact of micromechanics on the linewidth and chirp performance of MEMS-VCSELs," *IEEE J. Sel. Topics Quantum Electron.*, vol. 13, no. 2, pp. 367–373, Apr. 2007.

[13] S. Paul *et al.*, "Far-field, linewidth and thermal characteristics of a high-speed 1550-nm MEMS tunable VCSEL," *Opt. Express*, vol. 24, no. 12, p. 13142, Jun. 2016.

[14] W. De Cort, J. Beeckman, T. Claes, K. Neyts, and R. Baets, "Wide tuning of silicon-on-insulator ring resonators with a liquid crystal cladding," *Opt. Lett.*, vol. 36, no. 19, pp. 3876–3878, Sep. 2011.

[15] C. Levallois *et al.*, "Liquid crystal-based tunable photodetector operating in the telecom C-band," *Opt. Express*, vol. 26, no. 20, Sep. 2018, Art. no. 25952.

[16] Y. Xie, J. Beeckman, W. Woestenborghs, K. Panajotov, and K. Neyts, "VCSEL with photo-aligned liquid crystal overlay," *IEEE Photon. Technol. Lett.*, vol. 24, no. 17, pp. 1509–1512, Sep. 2012.

[17] O. Castany, L. Dupont, A. Shuaib, J. P. Gauthier, C. Levallois, and C. Paranthoën, "Tunable semiconductor vertical-cavity surface-emitting laser with an intracavity liquid crystal layer," *Appl. Phys. Lett.*, vol. 98, no. 16, Apr. 2011, Art. no. 161105.

[18] L. Frasunkiewicz, T. Czyszanowski, H. Thienpont, and K. Panajotov, "Electrically tunable VCSEL with intra-cavity liquid crystal: Design, optimization, and analysis of polarization- and mode-stability," *Opt. Commun.*, vol. 427, pp. 271–277, Nov. 2018.

[19] B. Sadani *et al.*, "Liquid-crystal alignment by a nanoimprinted grating for wafer-scale fabrication of tunable devices," *IEEE Photon. Technol. Lett.*, vol. 30, no. 15, pp. 1388–1391, Aug. 1, 2018.

[20] F. Taleb *et al.*, "Enhancement of VCSEL performances using localized copper bonding through silicon vias," *IEEE Photon. Technol. Lett.*, vol. 29, no. 13, pp. 1105–1108, Jul. 1, 2017.

[21] J. Li, S.-T. Wu, S. Brugioni, R. Meucci, and S. Faetti, "Infrared refractive indices of liquid crystals," *J. Appl. Phys.*, vol. 97, pp. 073501-1–073501-5, Mar. 2005.

[22] C. Belmonte *et al.*, "Optimization of electrically tunable VCSEL with intracavity nematic liquid crystal," *Opt. Express*, vol. 23, no. 12, p. 15706, Jun. 2015.

IEEE Proof